WFIRST coronagraph detector trap modeling results and improvements

Conference or Workshop Item

WFIRST coronagraph detector trap modeling results and improvements

Robert Effinger, Bijan Nemati, Maxime Rizzo, Patrick Morrissey, Leon Harding, et al.

Robert Effinger, Bijan Nemati, Maxime Rizzo, Patrick Morrissey, Leon Harding, Michael Bottom, Donald Pontrelli, Richard Demers, Nathan Bush, David Hall, Andrew Clarke, Andrew Holland, "WFIRST coronagraph detector trap modeling results and improvements," Proc. SPIE 10709, High Energy, Optical, and Infrared Detectors for Astronomy VIII, 1070917 (6 July 2018); doi: 10.1117/12.2311408

SPIE.

Event: SPIE Astronomical Telescopes + Instrumentation, 2018, Austin, Texas, United States

WFIRST Coronagraph Detector Trap Modeling Results and Improvements

Robert Effinger*[a], Bijan Nemati[b], Maxime Rizzo[c], Patrick Morrissey[a], Leon Harding[a], Michael Bottom[a], Donald Pontrelli[d], Richard Demers[a], Nathan Bush[e], David Hall[e], Andrew Clarke[e], Andrew Holland[e]

[a]Jet Propulsion Laboratory, California Institute of Technology, 4800 Oak Grove Drive, M/S-321-100, Pasadena, CA 91109; [b]Center for Applied Optics, University of Alabama in Huntsville, 301 Sparkman Dr., OPB400 Huntsville, AL 35899; [c]NASA Goddard Space Flight Center, Greenbelt, MD 20771; [d]Department of Mechanical Engineering, Villanova University, 800 E. Lancaster Ave, Villanova, PA 19085; [e]e2v Center for Electronic Imaging (CEI), the Open University, Milton Keynes, U.K.

ABSTRACT

The WFIRST coronagraph is being designed to detect and characterize mature exoplanets through the starlight reflected from their surfaces and atmospheres. The light incident on the detector from these distant exoplanets is estimated to be on the order of a few photons per pixel per hour. To measure such small signals, the project has baselined the CCD201 detector made by e2v, a low-noise and high-efficiency electron-multiplying charge-coupled device (EMCCD), and has instituted a rigorous test and modeling program to characterize the device prior to flight. An important consideration is detector performance degradation over the proposed mission lifetime due to radiation exposure in space. To quantify this estimated loss in performance, the project has built a detector trap model that takes into account detailed trap interactions at the sub-pixel level, including stochastic trap capture and release, and the deferment of charge into subsequent pixels during parallel and serial clocking of the pseudo-two-phase CCD201 device. This paper describes recent detector trap model improvements and modeling results.

Keywords: WFIRST, coronagraph, exoplanet, detector, CCD, EMCCD, trap modeling

1. INTRODUCTION

The Wide Field Infrared Survey Telescope (WFIRST) is a NASA flagship observatory that is being designed to measure the expansion history of the Universe, and to search for exoplanets through microlensing and direct imaging techniques. The WFIRST Coronagraph Instrument (CGI) is a technology demonstration instrument on the WFIRST observatory that is designed to detect and characterize exoplanets through direct imaging of the starlight reflected from their surfaces and atmospheres. The expected flux on the CGI science detector from these distant exoplanets will be on the order of a few photons per pixel per hour. In addition, the WFIRST mission duration is 5 years in a halo orbit around the Sun-Earth L2 Lagrange point. This combination of factors highlights the technology need for a radiation damage tolerant, low-noise, high-efficiency photon-counting detector. To meet this need, the CGI has baselined the CCD201 electron-multiplying charge-coupled device (EMCCD) made by e2v and has instituted a rigorous test and modeling program [1,2], in order to characterize the device prior to flight.

This paper describes recent detector trap model improvements and modeling results. The model has been updated to include charge density based trap capture time constants, informed through detailed physics-based modeling of the sub-pixel gate geometry and charge potentials. The phenomenon of an electron being captured and released multiple times by the same trap was modeled as a discrete-time Markov chain and used to verify the accuracy of the trap model. Modeling experiments were performed to predict signal loss in the frame and serial clocking directions. Additional modeling experiments were performed to understand and characterize image artifacts such as streaks and hot pixels.

*robert.effinger@jpl.nasa.gov; Telephone: +1 (832) 396-9003

High Energy, Optical, and Infrared Detectors for Astronomy VIII, edited by Andrew D. Holland, James Beletic, Proc. of SPIE Vol. 10709, 1070917 · © 2018 SPIE
CCC code: 0277-786X/18/$18 · doi: 10.1117/12.2311408

1.1 Statistics of Trap Capture and Release

This section provides a brief overview of the statistics of trap capture and release, for a more detailed description, please see [2]. The physics of trap capture and release are well characterized as random and independent events (i.e. Poisson statistics), whose frequency of occurrence obey the probability density function of the exponential distribution:

$$f(t) = \frac{1}{\tau} e^{-t/\tau} \tag{1}$$

In the detector model, a trap's behavior is determined by its capture and release time constants, τ_c and τ_r, and the probability of a capture/release in a duration of time, t, which is expressed as the integral under the curve of (Equation 1) and is known as the cumulative distribution function of the exponential distribution:

$$P(t) = \int_0^t \frac{1}{\tau} e^{-t'/\tau} dt' = 1 - e^{-t/\tau} \tag{2}$$

The release time constant for each species of trap in a damaged CCD is measured experimentally through a technique called "trap pumping" [3]. There is no direct measurement approach for a trap's capture time constant, but it can be estimated [2] from the following expressions, which relate an electron's thermal velocity, v_{th}, to the time it will take to encounter a trap:

$$\tau_c = \frac{1}{\sigma v_{th} n_e} \qquad \text{and} \qquad v_{th} = \sqrt{\frac{3k_B T}{m_e^*}} \tag{3,4}$$

where:

σ = trap cross section
k_B = Boltzmann's constant
m_e^* = effective mass of electron in lattice = 0.26 m_e
T = temperature of CCD = 160 K
n_e = local electron density

Trap cross section, σ, is measured empirically for each species of trap, and CCD operating temperature, T, is held constant by using active thermal control. For each trap, the local electron density, n_e, varies at each phase of clocking as packets are transferred from gate to gate, and pixel to pixel, out of the detector. A key contribution of this paper is a pixel level physics model the CCD201 during each phase of clocking (described in Section 2.1) that accurately models n_e for small signal levels (from 1 to 10e-). The prior model implementation used a power law parameterization [4] to extrapolate packet volume at full capacity down to the packet size of interest. Trap species that have been experimentally verified to exist in the irradiated CCD201 [5] and their properties are summarized in Table 1. Each trap species has a proportionality constant, **a**, called the *defect scaling factor*, which defines its prevalence in the silicon lattice (i.e. traps/um^3) as a function of radiation exposure. This parameter is described in more detail in Section 2.1.

Table 1. Physical properties and types of traps present in the CCD201 after exposure to radiation.

Trap Species	σ (cm^2)	τ_e (s)	E (eV)	a
Si-A center	1E-14	3.95E-08	0.17	2.4
(V-V)--	5E-16	8.41E-05	0.21	0.27
Unknown	5E-16	0.35	0.3	0.29
Si-E center	5E-15	57	0.46	1.23

1.2 Detector Clocking

This section gives a brief overview of pseudo 2-phase parallel clocking in the e2v CCD201 detector, for a more detailed description, please see [2]. Figure 1 shows the CCD201 pseudo 2-phase architecture with four gate electrodes per pixel. An ion implant elevates the potential in every other electrode. Four quadrants are defined per pixel, Q1 through Q4, having the feature that the electric field points in the same direction throughout each quadrant making the sweep direction of any released electrons straightforward to model.

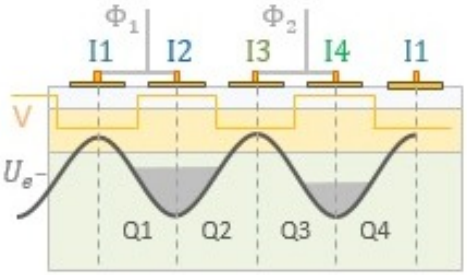

Figure 1. CCD201 pseudo 2-phase architecture – Gate electrodes I1, I2, and I3, I4 are tied together to enable parallel clocking with two *inputs,* φ_1 *and* φ_2.

Clocking in the CCD201 is depicted in Figure 2, and can be described as a sequence of steps in which voltage inputs φ_1 and φ_2 are cycled repeatedly from high to low. During integration, φ_1 and φ_2 are held at the same voltage resulting in accumulation of charge into two packets per pixel, one under I2 and one under I4. In the combine step, φ_2 is high and φ_1 is low, moving charge from quadrants Q1,2 into Q3,4, which combines the two packets formed during integration. In the transition steps, φ_1 and φ_2 are simultaneously raised and lowered (or vice versa) resulting in a similar voltage profile to the integrate step. Finally, in the transfer step, φ_1 is high while φ_2 is low, transferring charge from quadrants Q3,4 into Q1,2. These steps are repeated until all charge packets are transferred from the frame into the serial register.

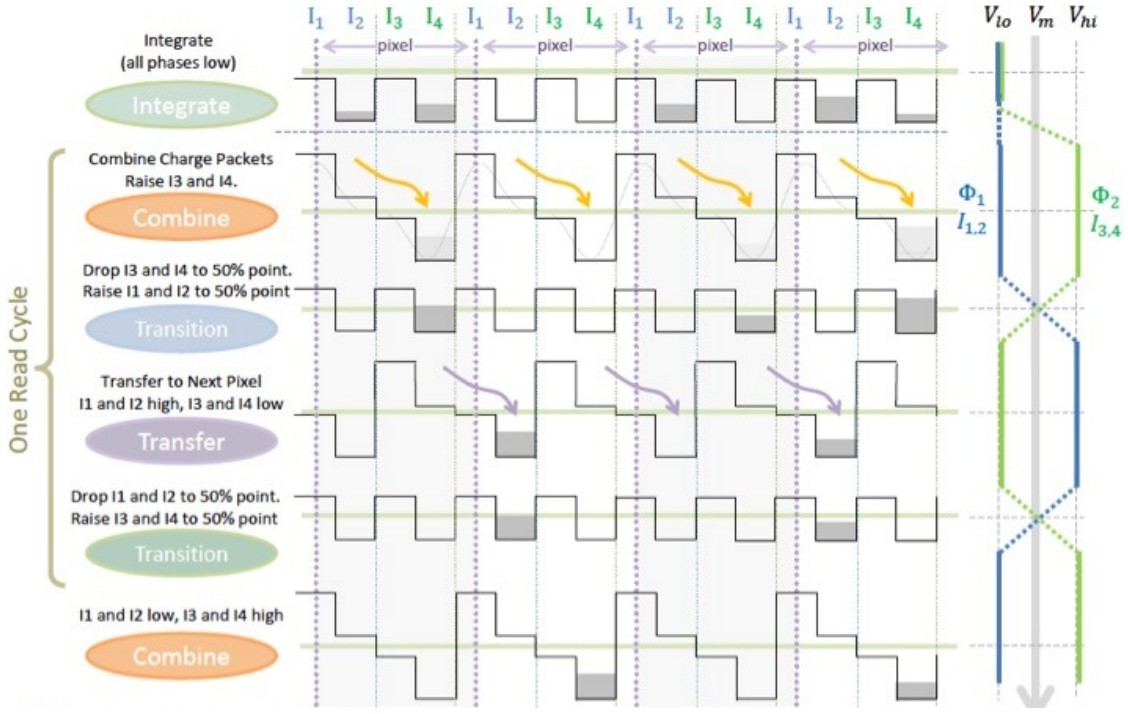

Figure 2. Pseudo 2-phase clocking in the e2v CCD201. Diagram based on original from Alice Reinheimer, e2v.

For trap modeling, the most important features of the clocking approach are captured in Table 2, which describes for each clocking step the rules for sweeping of released electrons, packet availability for electron capture, and the time duration for trap capture/release.

Table 2. Sweep and capture table

Clocking Step	Time Duration (s)	Sweep rules for released electrons		Rules for electron capture	
		Q1,2	Q3, 4	Q1,2	Q3,4
Integrate	100	Q1,2	Q3,4	Yes	Yes
Combine	2.5E-7	Q3,4	Q3,4	No	Yes
Transition	2.5E-7	Q1,2	Q3,4	Yes	Yes
Transfer	2.1E-4	Q1,2	Next pixel Q1,2	Yes	No

2. DETECTOR TRAP MODEL IMPROVEMENTS

2.1 Physics-based Packet-level Modeling

To accurately model trap capture and release it is important to have an accurate model of the charge packet location, size, and density at each phase of detector clocking. This is especially important at the small signal levels relevant to photon counting. In previous work, the Center for Electronic Imaging (CEI) at Open University has shown that pixel-level modeling of EMCCDs [6,7,8] is useful for determining potential profiles, charge storage volumes, and charge transfer paths in EMCCDs used in space telescope applications. In this section, we describe a pixel-level physics model of the CCD201 created by CEI for the WFIRST CGI, and we show how its predictions of charge packet geometry are incorporated into the detector trap model to improve modeling accuracy.

CEI used a commercial TCAD software package (SILVACO®) to create a pixel-level model of the CCD201 with characteristics such as gates, electrodes, and barrier implants. Shown in Figure 3, the TCAD model of the CCD201 image pixel is 13 μm square, and has four phases with barrier implants beneath I1 and I3. Additional electrodes are modeled on each side to isolate boundary effects. With a model of the pixel geometry in place, the electrical properties of the pixel were simulated for each clocking phase, giving rise to potential profiles and charge packet characteristics. A TCAD model was also developed for the serial register pixels of the CCD201, which are comprised of two distinct pixel geometries, the standard register pixel and the electron-multiplying (EM) register pixel.

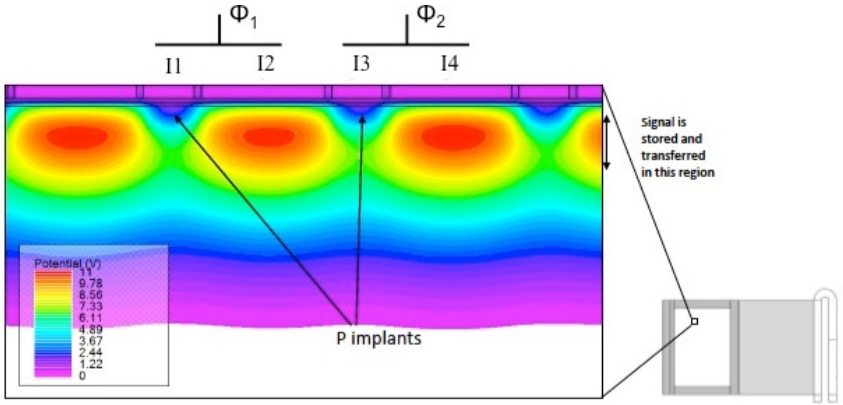

Figure 3. SILVACO TCAD model of the CCD201 image pixel depicted with a potential profile for the Integrate step.

The charge packet information generated by the TCAD model is incorporated into the detector trap model as a set of data files, one for each pixel type and clocking phase. Each file consists of a 3D grid of data points that sample the

charge packet density across the pixel at a resolution of 0.05 μm (see Figure 4), and for charge packet sizes ranging from 1 e- to 10 e-.

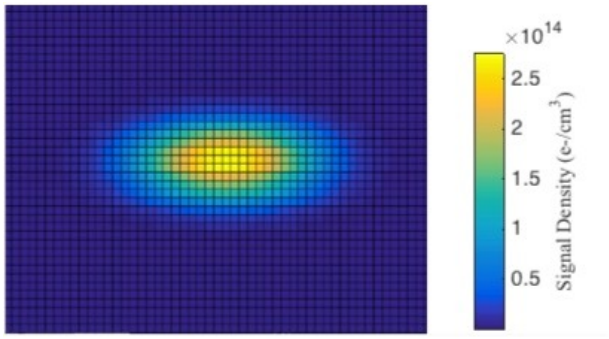

Figure 4. An example of the charge packet density information generated from the TCAD model. This figure depicts a 2D slice through a 3D data set of charge packet density at a grid resolution of 0.05 μm × 0.05 μm, for a 10e- charge packet in an image pixel during the integrate clocking step.

In order to randomly seed traps in the detector model, we need to know their density as a function of radiation dose. Trapping sites are caused by irradiated particles colliding with and creating defects in the silicon lattice. These defects appear linearly with radiation dose (Equation 5), each trap having a unique proportionality constant, ***a***, that depends on the concentration of impurities in the silicon lattice indicative of that trap species (see Table 1).

$$N_t(cm^{-3}) = a \cdot NIEL(keV cm^{-2} g^{-1}) \cdot \phi(cm^{-2}) \quad (5)$$

where:

$N_t =$ number of traps per unit volume
$a =$ scaling factor (unique to each defect type)
$NIEL =$ non-ionising energy loss of a particle with given energy
$\phi =$ the delivered fluence at the same energy

The detector trap model seeds traps throughout the detector in both the frame area and serial register by randomly assigning each trap an (x, y, z) location at a resolution of 0.05 μm, and with the abundance specified by Equation 5. For each seeded trap, the probability of capture and release during each phase of clocking is pre-computed for charge packet sizes from 1 to 10e- using Equations 2, 3, and 4, and the following inputs: (1) $n_e =$ local electron density (from the TCAD data files), and (2) $t =$ time duration of the clock phase (from Table 2). Then, in order to improve detector model runtime, if a trap doesn't have at least 1% probability of capture during at least one clocking phase, it is removed.

2.2.1 Narrow Channel-width Modeling

A design modification to the CCD201 that could reduce charge transfer inefficiency (CTI) at the expense of full-well capacity is to narrow the channel-width in the frame area of the device. It is hypothesized that by narrowing the channel width, the electron charge cloud is compressed, and therefore encounters less traps during clocking.

To test this hypothesis, CEI developed TCAD models of charge packet density for three channel widths, $\{2, 4, \text{and } 9\}$ μm (shown in Figure 5). The charge packet density data was then imported into the detector trap model to estimate the improvement in performance (shown in Figure 6). For this experiment, a point source (a simulated planet) was placed on the detector in the middle of the frame area such that the planet signal is clocked through 522 frame pixels until it reaches the serial register. The experiment was repeated 100 times at each of three source flux levels, and three channel widths. A clear improvement in CTI is seen between the 9 and 4 μm cases, with little further improvement at 2 μm. Another useful metric is the average number of traps (with greater than 1% probability of capture) that exist

between the source signal and the serial register (Figure 7). In theory, the number of traps that exist between the source signal and the SR will be directly correlated with CTI. Figure 7 shows that at narrower channel widths, the source signal sees significantly fewer traps.

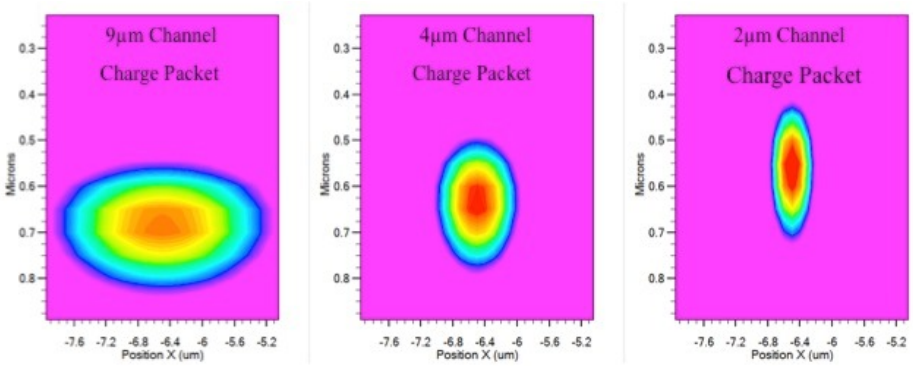

Figure 5. Charge packet geometry for three simulated channel widths.

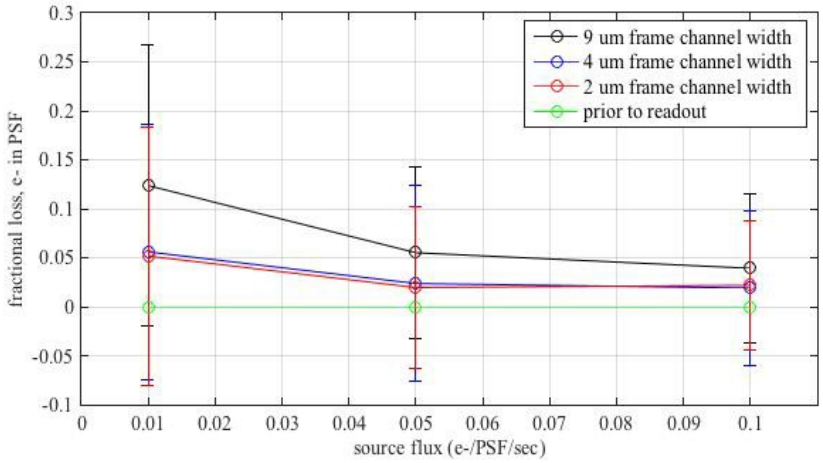

Figure 6. CTI vs. source flux for three simulated channel widths.

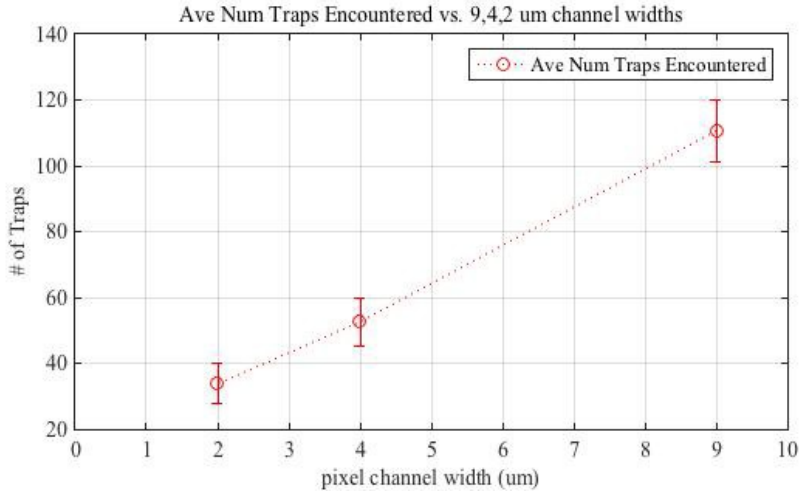

Figure 7. Average number of traps that exist between the source signal and serial register vs. channel width.

2.2 Modeling trap capture and release as a Discrete-time Markov chain

The goal of this section is to develop an analytical model of detector trap state evolution that accounts for the probability that a trap may capture and release an electron multiple times from the same electron packet, and then use it to determine the accuracy of the current detector trap model implementation.

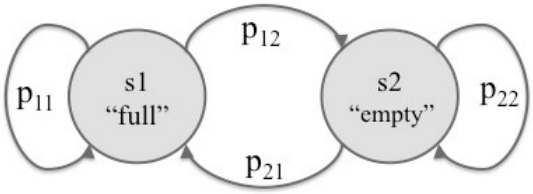

Figure 8. Directed-graph representation of a trap modeled as a Discrete-Time Markov Chain [9]. The trap can be either "full" or "empty" and the transitions between those states occur with probabilities that depend only on the present state.

2.2.1 Specification of Discrete-Time Markov Chain [9]:

- Discrete State Space (s1,s2,…)
  - Satisfies the Markov property, the probability of moving to the next state depends only on present state

$$\Pr\left(X_{n+1}=x \middle| X_1=x_1, X_2=x_2, \square\ , X_n=x_n\right)=\Pr\left(X_{n+1}=x \middle| X_n=x_n\right) \tag{6}$$

  - States are represented as vertices in a directed graph (Figure 8).
- State Transitions (p_{11},p_{12},…)
  - Probability of going from one state at time ***n***, to another at time ***n+1***
  - Transitions are represented as edges in a directed graph (Figure 4), or as a transition matrix, ***P***

$$P=\begin{bmatrix} p_{11} & p_{12} \\ p_{21} & p_{22} \end{bmatrix} \tag{7}$$

- The distribution over states can be written as a stochastic row vector, ***x***,
  - $\boldsymbol{x^{(n+1)}=x^{(n)}P}$, such that ***k*** time periods later, $\boldsymbol{x^{(n+k)}=x^{(n)}P^k}$
  - For example, if at time ***n*** a trap is in state $\boldsymbol{s_1}$ ("full"),

$$x^{(n)}=\begin{bmatrix} 1 & 0 \end{bmatrix} \tag{8}$$

  - Then at time ***k*** the distribution over trap states is:

$$x^{(n+k)}=\begin{bmatrix} 1 & 0 \end{bmatrix}\begin{bmatrix} p_{11} & p_{12} \\ p_{21} & p_{22} \end{bmatrix}^k \tag{9}$$

2.2.2 An Example Calculation

Assume a (V-V)-- trap in Q1,2 during the frame transfer clocking step such that an electron packet stays above the trap for 0.21 milliseconds (Table 2). Also assume that the charge packet has 10e-, and that the trap is located near the center of the charge packet, such that the local electron density is 1E19 e-/m^3.

- Frame transfer step duration, $T_{transfer} = 210\ us$ (from Table 2)
- Emission time constant, $\tau_e = 84.1\ us$ (from Table 1)
- Capture time constant, $\tau_c = 12.0\ us$ (from Equations 3,4 and Table 1)

In order to simulate trap behavior as a discrete-time Markov chain, it is important to choose a discrete simulation time step that is smaller than the timescales of interest. Here we choose $\Delta t = 1\ us$. Note that in some detector clocking steps the simulation time step will need to be set to a smaller value (e.g. $1\ ns$). Now, we compute the probabilities of capture and release during a single simulation time step, Δt:

- Discrete simulation timestep, $\Delta t = 1\ us$
- $P_{12} = 1 - e^{(-\Delta t/\tau_e)} = 0.0118$
- $P_{21} = 1 - e^{(-\Delta t/\tau_c)} = 0.0800$
- $P_{11} = 1 - P_{12} = 0.9882$
- $P_{22} = 1 - P_{21} = 0.9200$

Now compute the probability that the trap is full or empty at the end of the transfer clocking step by taking the starting state of the trap, either $x_{start} = [1 \quad 0]$ for full, or $x_{start} = [0 \quad 1]$ for empty, and multiplying by the state transition equation (Equation 9).

- $T_{transfer} = 210 * \Delta t$
- $x_{end} = x_{start} \begin{bmatrix} 0.9882 & 0.0118 \\ 0.0800 & 0.9200 \end{bmatrix}^{210} = [0.8712 \quad 0.1288]$

Note that x_{end} does not depend on x_{start} once the stochastic system reaches a steady state. In this example, there is an 87.1% chance the trap will be full (and 12.9% chance of empty) at the end of the clocking step independent of whether the starting state of the trap was full or empty.

2.2.3 Comparison with current detector trap model implementation

Rather than modeling trap behavior as a discrete-time Markov chain, the current detector trap model implementation makes a simplifying assumption, notably that there is not enough time for a trap to release an electron twice during a single clocking step. Therefore, during a single clocking step, each trap has the chance to release and capture, but must wait until the next clocking step to re-release. It is a good assumption for clocking steps with a fast duration since the likelihood of multiple captures and releases becomes vanishingly small. However, the simplified approach leaves room for error when both capture and release time constants are small relative in comparison to the clocking step duration, as is the case for some trap species in the integrate and transfer clocking steps. Mathematically, the simplifying assumption can be represented as the following equation.

$$x_{(n+k)} = x_n {M_{rel}}^k {M_{cap}}^k = x_n \begin{bmatrix} p_{11} & p_{12} \\ 0 & 1 \end{bmatrix}^k \begin{bmatrix} 1 & 0 \\ p_{21} & p_{22} \end{bmatrix}^k \tag{10}$$

M_{rel} represents the release time step with no possibility of capture, while M_{cap} represents the capture time step with no possibility of release. This order of matrix operations requires that all of the release simulation time steps occur before any of the capture simulation time steps. Due to this sequential order of operations, the simplified approach can

overestimate the likelihood that a trap will end up full at the end of a clocking step. For example, taking the sample calculation provided above, the simplified approach results in a calculated probability of 100% that the trap is full at the end of the clocking step, an error of 13.4%.

- $x_{end} = x_{start}\begin{bmatrix} 0.9882 & 0.0118 \\ 0 & 1 \end{bmatrix}^{210}\begin{bmatrix} 1 & 0 \\ 0.0800 & 0.9200 \end{bmatrix}^{210} = [1.0 \quad 0.0]$

Table 3 summarizes a comparative analysis of the Discrete-time Markov chain (DTMC) approach and the current detector trap model implementation, denoted here as the "Simplified" approach. This analysis computes the probability that a trap will be full at the end of a specified clocking step, given a starting condition of full. The analysis is repeated over a range of clocking steps {integrate, combine, transition, transfer}, trap species {Si-A, (V-V)--, Unknown, and Si-E)}, and capture time constants {10ns, 1000ns}. Note that semiGate 1 refers to Q1,2 in Table 2, while semiGate 2 refers to Q3,4. For brevity, the results for semiGate = 2 were omitted from Table 3, because they are very similar to the results for semiGate = 1. Rows are highlighted in grey where the two approaches differ in prediction by more than 1%. Notably, only the Si-A trap species, which has a very fast release time constant, is poorly predicted by the "Simplified" trap model implementation. In practice, however, this limitation of the current approach doesn't matter much because trap species with very fast release times, such as Si-A, do not have much of an effect on image degradation, as described in Section 3.X. Note that an Si-A trap in semiGate 1 (Q1,2) has a zero probability of being "full" at the end of the combine step because it has a fast release time constant, and the released electron is immediately swept from Q1,2 into Q3,4 (Table 2). The other three trap species remain full during the combine step, however, because their release time constants are orders of magnitude larger than the step's time duration.

Table 3. Comparative analysis of Discrete-time Markov chain (DTMC) approach to current detector trap model approach

Probability that X(n+k) = "Full" given X(n) = "Full"					Tau_cap = 10 ns		Tau_cap = 1000 ns	
					DTMC	Simplified	DTMC	Simplified
Frame Step	Step Time (ns)	Trap Species	Tau_rel (ns)	semiGate (1 or 2)	P_full	P_full	P_full	P_full
integrate	1E+10	Si-A	39.5	1	0.79	1.00	0.04	1.00
integrate	1E+10	(V-V)--	84100	1	1.00	1.00	0.99	1.00
integrate	1E+10	Unknown	3.54E+08	1	1.00	1.00	1.00	1.00
integrate	1E+10	Si-E	5.7E+10	1	1.00	1.00	1.00	1.00
combine	250	Si-A	39.5	1	0.00	0.00	0.00	0.00
combine	250	(V-V)--	8.41E+04	1	1.00	1.00	1.00	1.00
combine	250	Unknown	3.54E+08	1	1.00	1.00	1.00	1.00
combine	250	Si-E	5.7E+10	1	1.00	1.00	1.00	1.00
transition	250	Si-A	39.5	1	0.79	1.00	0.04	0.22
transition	250	(V-V)--	84100	1	1.00	1.00	1.00	1.00
transition	250	Unknown	3.54E+08	1	1.00	1.00	1.00	1.00
transition	250	Si-E	5.7E+10	1	1.00	1.00	1.00	1.00
transfer	2.12E+05	Si-A	39.5	1	0.79	1.00	0.04	1.00
transfer	2.12E+05	(V-V)--	84100	1	1.00	1.00	0.99	1.00
transfer	2.12E+05	Unknown	3.54E+08	1	1.00	1.00	1.00	1.00
transfer	2.12E+05	Si-E	5.7E+10	1	1.00	1.00	1.00	1.00

This analysis indicates that the current detector trap model approach is sufficiently accurate to model radiation-induced trap behavior in the CCD201. However, it also indicates the need for a more accurate approach, such as DTMC, if any of the trap species have release and capture time constants that are on the same order of magnitude and small relative to the clocking cycle. A DTMC analysis of the serial register was performed as well, but omitted here, because the serial register has been shown to have negligible effects on signal degradation at fast clocking speeds (see Section 3.2), such as those specified in Table 2.

3. MODELING EXERIMENTS

Two separate modeling experiments were performed in order to predict signal loss in the frame and serial clocking directions, independently, over a range of flux levels. The model parameters for these experiments are described in Section 3.1, and the results are summarized in Sections 3.2 and 3.3. Section 3.4 discusses image artifacts in the modeled results such as hot pixels and streaks.

3.1 Detector Model Parameters

The detector model parameters were chosen in order to be representative of the WFIRST flight environment, and the WFIRST CGI flight detector timing and noise requirements. Detector trap densities were seeded in accordance with Table 1 and a WFIRST mission lifetime of 6 years (WIRST mission lifetime was reduced to 5 years after this experiment was performed). The detector clocking parameters were set in accordance with Table 2. Detector noise parameters were chosen to be consistent with instrument requirements at the time the modeling experiment was performed. (e.g. dark current = 1.3e-4 e/pix/sec, and CIC = 1.2e-2 e-/pix/frame) The source PSF was assumed to have a Gaussian distribution with a FWHM of 3 pixels across, and its intensity was varied from 0.1 e-/PSF/sec to 0.001 e-/PSF/sec, which encompasses the range of expected CGI science targets. A frame integration time of 100 seconds was assumed in order to balance the impacts of cosmic rays, detector noise properties, and radiation trapping effects. These experiments did not include residual background light from the coronagraph, however, that would be present in actual science frames (often referred to as speckles). An EMCCD with 9um channel width was assumed, because the modified devices with narrow channel width have not yet been fabricated and tested in the lab.

3.2 Signal Loss in the Serial Register

For this experiment, the PSF was placed at the very bottom and left side of the detector (assuming the detector readout direction is down and to the right), such that the source signal only travels through a few pixels in the frame area, but travels through the entire length of the serial register. The results are presented in Figure 9. Due to fast clock timing in the serial direction, traps seeded in the serial registers have minimal effect on charge transfer efficiency, less than 1%. This is consistent with lab experiments that show the same behavior.

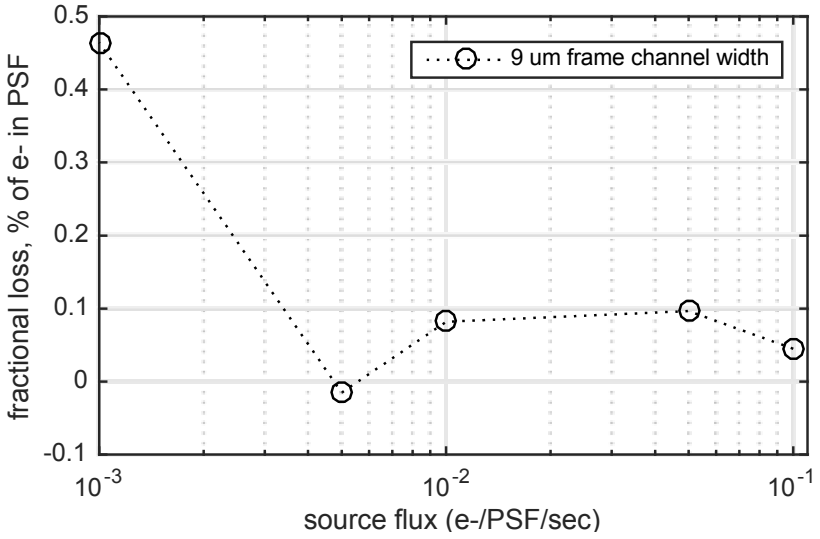

Figure 9. Signal loss in the serial register due to radiation-induced traps.

3.3 Signal Loss in the Frame Area

For this experiment, the PSF was placed in the middle of the 1024x1024 detector array. The PSF, therefore, traveled through 512 frame pixels before reaching the serial register. In addition, the effects due to serial register clocking were disabled. The fractional loss of electrons from the PSF core was measured for a range of flux levels, [0.1, 0.05, 0.01, 0.005, 0.0025, 0.001] e-/PSF/sec, and the results are shown in Figure 10. A strong dependence between source flux and fractional loss of e- in the PSF is demonstrated in the frame area. This is also consistent with lab experiments.

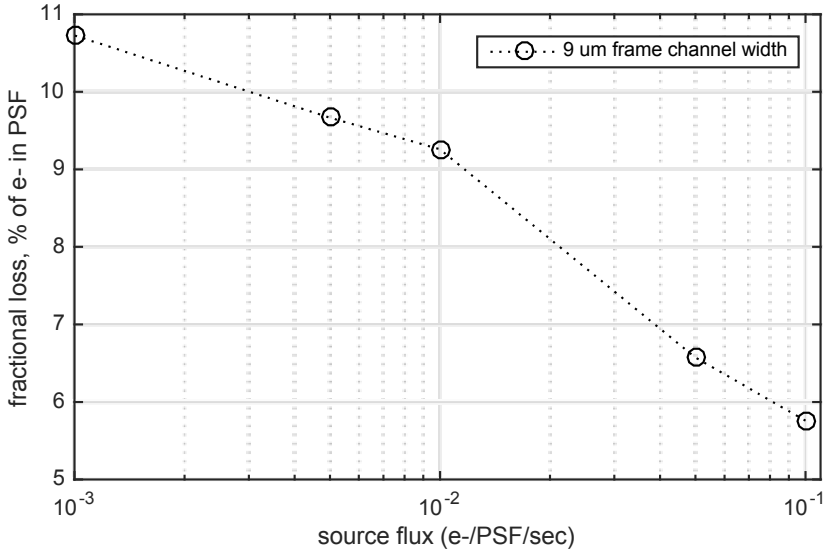

Figure 10. Signal loss in the frame area due to radiation-induced traps.

3.4 Image Artifacts – Streaks and Hot Pixels

One interesting aspect of the detector trap model is that image artifacts such as hot pixels and streaks show up in the aggregated frame. Figure 11 shows an interesting experiment where an artificial source signal (a line of light) is placed horizontally across the middle of a 900x100 pixel detector. The top 100 frame pixels are assumed to be detector over scan. The artificial source signal was placed at pixel row 500 and varied from 0.1 to 0.001 e-/PSF/sec. The frames were integrated until the source signal in each row reached a certain number of electrons (e.g. 40 e-). This means that for the fainter source signals, many more frames were aggregated leading to a greater number of background electrons in the frame, and also more image artifacts. Hot pixels as well as streaks were evident in the modeling results, consistent with laboratory experiments.

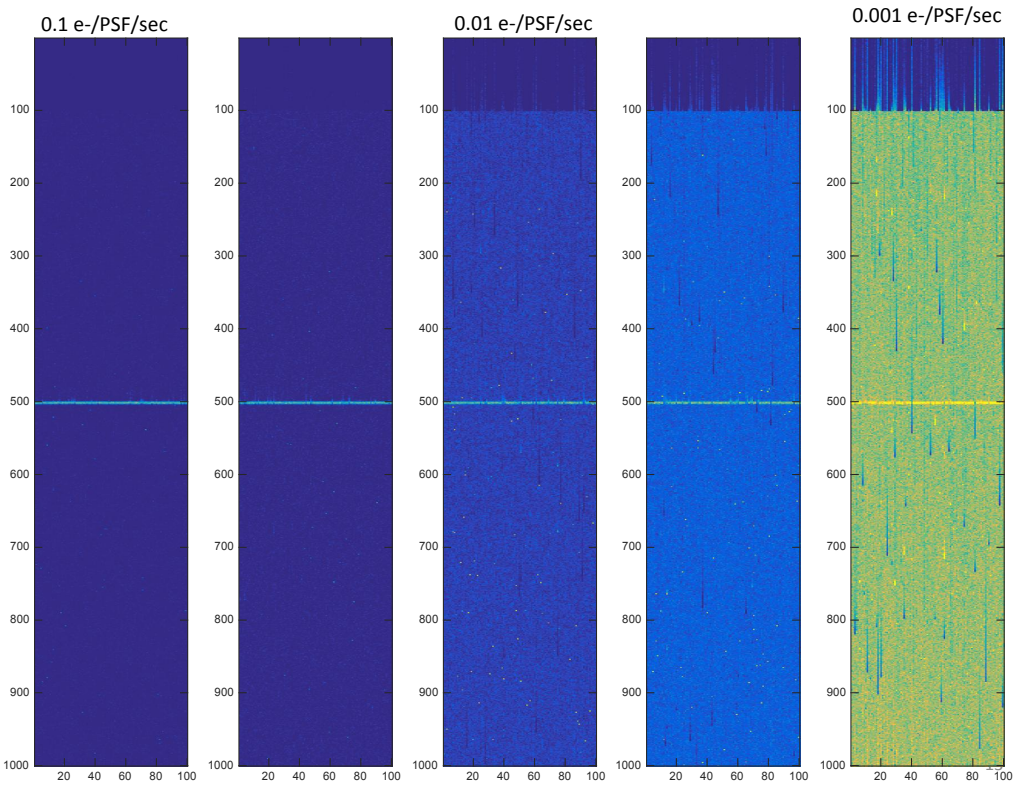

Figure 11. Detector model experiments at varying target flux levels. The source signal is simulated as a 2D Gaussian PDF in each of 100 columns with the mean of the PSF at pixel row 500. Frames are integrated at 100sec each until the source signal reaches ~500 e- per column (e.g. each 2D PSF). Features such as hot pixels and streaks are more pronounced in the integrated frame with increasing integration time.

4. CONCLUSIONS

The WFIRST CGI is designed to detect and characterize exoplanets through the starlight reflected from their surfaces and atmospheres. In order to detect such extremely dim science targets, the CGI needs a radiation tolerant, low-noise, and high-efficiency, photon-counting detector. To this aim, the WFIRST CGI has instituted a rigorous test and modeling program to characterize the CCD201-20 detector made by e2v. This paper describes recent detector trap model improvements and modeling results. The model has been updated to include charge density based trap capture time constants, informed through detailed physics-based modeling of the sub-pixel gate geometry and charge potentials. In addition, the phenomenon of an electron being captured and released multiple times by the same trap was modeled as a discrete-time Markov chain and used to verify the accuracy of the trap model. Modeling experiments were performed to predict signal loss in the frame and serial clocking directions. Additional modeling experiments were performed to understand and characterize image artifacts such as streaks and hot pixels.

REFERENCES

[1] Harding, L. et al., "Technology advancement of the CCD201-20 EMCCD for the WFIRST coronagraph instrument: sensor characterization and radiation damage", J. Astron. Telesc. Instrum. Syst. 2(1), 011007 (2016).

[2] Nemati, B., et al., "The effect of radiation induced traps on the WFIRST coronagraph detectors", Proc. SPIE 9915, High Energy, Optical, and Infrared Detectors for Astronomy VII, 99150M (1 August 2016); doi: 10.1117/12.2235278.

[3] Bush, N., et al., "Development of in-situ trap characterization techniques for Electron Multiplying CCDs", prepared for submission to JINST.

[4] Short, A., et al., "A fast model of radiation-induced electron trapping in CCDs for implementation in the Gaia data processing." Proc. SPIE 7742, High Energy, Optical, and Infrared Detectors for Astronomy IV, 774212 (July 16, 2010); doi: 10.1117/12/856386.

[5] D. Hall et al. , "Studying defects in the silicon lattice using CCDs", Journal of Instrumentation, Volume 9, Issue 12, article id. C12004 (2014).

[6] G. Seabroke, et al., "Silvaco ATLAS model of ESA's Gaia satellite e2v CCD91-72 pixels", Proc. SPIE, 7742(2010).

[7] Bush, N., et al., Simulations of charge transfer in Electron Multiplying Charge Coupled Devices. *Journal of Instrumentation*, 9(12), article no. C12042.

[8] Clarke, A., et al., "Device modelling and model verification for the Euclid CCD273 detector" Proc. SPIE 8453(2012).

[9] Bertsekas, D., and Tsitsiklis, J., *Introduction to Probability*. 2nd ed. Athena Scientific, 2008. ISBN: 9781886529236.